IEEE INFOCOM 2021 - IEEE Conference on Computer Communications | 978-1-6654-0325-2/21/$31.00 ©2021 IEEE | DOI: 10.1109/INFOCOM42981.2021.9488836

Statistical Delay and Error-Rate Bounded QoS Provisioning for 6G mURLLC Over AoI-Driven and UAV-Enabled Wireless Networks

Xi Zhang†, Jingqing Wang†, and H. Vincent Poor‡

†Networking and Information Systems Laboratory
Department of Electrical and Computer Engineering, Texas A&M University, College Station, TX 77843, USA
‡Department of Electrical Engineering, Princeton University, Princeton, NJ 08544, USA
E-mail: {*xizhang@ece.tamu.edu*, *wang12078@tamu.edu*, *poor@princeton.edu*}

***Abstract*—Massive ultra-reliable and low latency communications (mURLLC) has been developed as a new and dominating 6G standard traffic service to support statistical delay and error-rate bounded quality-of-services (QoS) provisioning for real-time data-transmissions. Inspired by mURLLC, finite blocklength coding (FBC) has been proposed to upper-bound both delay and error-rate by using short-packet data communications. On the other hand, to solve the massive connectivity problem imposed by mURLLC, the unmanned aerial vehicle (UAV)-enabled systems are developed by leveraging their deploying flexibility and high probability of establishing line-of-sight (LoS) wireless links while guaranteeing various QoS requirements. In addition, the age of information (AoI) has recently emerged as a new QoS performance metric in terms of information freshness. However, how to efficiently integrate and implement the above new techniques for statistical delay and error-rate bounded QoS provisioning over 6G standards has neither been well understood nor thoroughly studied. To overcome these challenges, we propose the statistical delay and error-rate bounded QoS provisioning schemes which leverage the AoI technique as a key QoS performance metric to efficiently support mURLLC over UAV-enabled 6G wireless networks in the finite blocklength regime. Specifically, first, we develop the UAV-enabled 3D wireless networking models with wireless-link channels using FBC. Second, we build up the AoI-metric based modeling frameworks in the finite blocklength regime. Third, taking into account the peak AoI violation probability, we formulate and solve the AoI-driven ϵ-effective capacity maximization problems to support statistical delay and error-rate bounded QoS provisioning. Finally, we conduct the extensive simulations to validate and evaluate our developed schemes.**

***Index Terms*—Statistical delay and error-rate bounded QoS, UAV-enabled communications, 6G mURLLC, AoI-driven ϵ-effective capacity, FBC, 3D wireless channel.**

I. Introduction

THE DELAY-BOUNDED quality-of-services (QoS) theory [1] [2] [3] has been proposed as a promising technique to support the explosively growing demands of time-sensitive wireless multimedia applications over 5G and the upcoming 6G multimedia mobile wireless networks. Due to the highly time-varying nature of wireless fading channels, researchers have proposed the concept of *statistical QoS provisioning* [4] [5], in terms of effective capacity [6] and delay-bounded violation probabilities, in supporting delay-sensitive multimedia wireless services over 6G mobile wireless networks.

Towards this end, as one of the 6G standard traffic services, *massive Ultra-Reliable Low-Latency Communications (mURLLC)* [7] have been proposed to quantitatively design and evaluate various QoS performances. Researchers have proposed and investigated the short-packet data communication techniques, such as finite blocklength coding (FBC) [8], in supporting stringent QoS requirements of 6G mURLLC for time-sensitive wireless services. The authors of [9] have shown that the codeword blocklength can be as short as 100 channel symbols for reliable communications. The authors of [10] have studied different properties of channel codes that approach the fundamental limits of a given memoryless wireless channel using FBC.

On the other hand, one of the major challenges for ensuring the stringent QoS requirements of 6G mURLLC is the massive connectivity problem. While most of the previous research works for 6G mURLLC focus on investigating the short-packet data transmissions between ground devices and ground base station (GBS). However, it is difficult to support the stringent 6G mURLLC requirements by a single wireless link between the mobile devices and the GBS. Therefore, unmanned aerial vehicles (UAVs) can be utilized to support time-sensitive wireless services for addressing the massive connectivity problem caused by 6G mURLLC. Due to its deployment capability, high mobility, and high probability of establishing line-of-sight (LoS) communications, UAV is ideal for supporting 6G mURLLC to upper-bound both delay and error-rate [11]. The authors of [12] have investigated the average achievable data rate of the control information delivery from the GBS to UAV using a 3D channel model. A model for beyond visual line-of-sight (BVLOS) operation by using finite-blocklength piloting signals for UAVs has been developed in [13]. The authors of [14] have jointly optimized the blocklength allocation and

The work of Xi Zhang and Jingqing Wang was supported in part by the U.S. National Science Foundation under Grants CCF-2008975, ECCS-1408601, and CNS-1205726, and the U.S. Air Force under Grant FA9453-15-C-0423. The work of H. Vincent Poor was supported in part by the U.S. National Science Foundation under Grants CCF-0939370 and CCF-1908308.

the UAV's location to minimize the decoding error probability subject to the latency requirement.

In addition, the age of information (AoI) has recently emerged as the new dimension of QoS performance metric in terms of the freshness of aggregated data measurements from source devices when they reach the remote destination devices, especially for UAV-enabled applications, such as UAV-enabled wireless sensor networks. The concept of AoI [15] [16] [17] has recently emerged as the new dimension of QoS performance metric to quantitatively measure the freshness of information that a receiver has about the status of a remote source. The authors of [18] have studied the age-optimal trajectory planning problem in UAV-enabled wireless sensor networks. The authors of [19] have formulated and solved an optimization problem to jointly optimize the UAV's flight trajectory as well as energy and service time allocations for data packet transmissions. A joint sensing time, transmission time, UAV trajectory, and task scheduling optimization problem has been investigated in [20] to minimize the AoI function.

Furthermore, the design and analysis of short-packet communications when considering the AoI metric for UAV-enabled systems are of great importance because the status updates normally consist only of a small number of information bits and needed to be delivered to the destination as fast as possible. Towards this end, the FBC based AoI measurement has been proposed for analyzing the 6G mURLLC-enabled UAV systems while measuring the freshness of the collected data by using short-packet data communications. The authors of [21] have analyzed the benefits of channel coding on AoI in broadcast networks. The authors of [22] have studied the impact of the channel coding blocklength on the freshness of data in a status-update first-come first-serve (FCFS) queueing system for reliable transmissions. However, there is only a limited number of research works focusing on the FBC based AoI analyses over UAV-enabled wireless networks. As a result, how to efficiently integrate and implement the above new techniques for statistical delay and error-rate bounded QoS provisioning over 6G standards has neither been well understood nor thoroughly studied.

To effectively overcome the above-mentioned challenges, in this paper we propose to develop the statistical delay and error-rate bounded QoS provisioning schemes which leverage the AoI technique as a key QoS performance metric in supporting mURLLC over UAV-enabled 6G wireless networks in the finite blocklength regime. In particular, we develop UAV-enabled wireless networking models with 3D wireless channel and the channel coding rate model in the finite blocklength regime. Then, we build up the AoI-metric based modeling frameworks for supporting UAV-enabled 6G mURLLC services using FBC. Taking into account the peak AoI violation probability, we formulate and solve the AoI-driven ϵ-effective capacity maximization problems to support statistical delay and error-rate bounded QoS provisioning over AoI-driven and UAV-enabled 6G wireless networks. Simulation results are included, which evaluate and validate our proposed schemes to support statistical delay and error-rate bounded QoS provisioning.

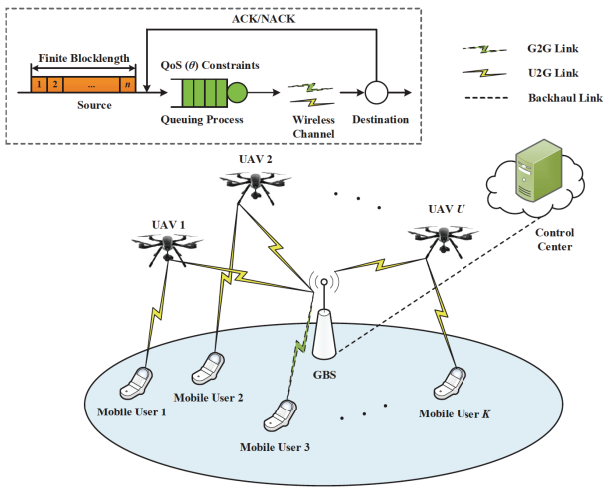

Fig. 1. The system architecture model for FBC based AoI-driven and UAV-enabled wireless networks, where the source device generates a status update packet with blocklength n once it receives an ACK from the destination device, implying that the previous status update packet is successfully decoded at the destination. G2G and G2U links represent the ground-to-ground link and ground-to-UAV link, respectively.

The rest of this paper is organized as follows: Section II establishes FBC based UAV based wireless networking models. Section III builds up the AoI-metric based modeling frameworks for 6G mURLLC using FBC. Section IV formulates and solves the AoI-driven ϵ-effective capacity maximization problem for both delay and error-rate bounded QoS provisioning in supporting 6G mURLLC in the finite blocklength regime. Section V validates and evaluates the system performance for our proposed schemes. The paper concludes with Section VI.

II. The System Models

Consider a FBC based UAV-enabled system architecture model, which consists of U UAVs, K mobile users and one GBS, as shown in Fig. 1. We assume that the GBS, mobile device, and UAV are equipped with single antenna. Without loss of generality, we assume that all K mobile devices are randomly distributed in a circle and the GBS is located at the center of the circle. Due to the obstruction of buildings on the ground, the channel quality between the mobile devices and the GBS may not be good enough for supporting the stringent requirements of 6G mURLLC. Towards this end, we consider that there are U UAVs deployed over the area to meet the stringent delay and error-rate bounded QoS requirements for 6G mURLLC. For the sake of simplicity, we consider there are N time instants. In each time instant l $(l = 1, \ldots, N)$, we assume that the mobile device generates a status update packet, which contains fixed M bits of information. By using FBC, we can then encode the status update packet into a codeword with n channel uses. In addition, assume that the locations of the UAVs and mobile devices can be obtained in advance by using the Global Positioning System (GPS). For simplicity, we denote the 3D position of the GBS as $\boldsymbol{q}_{\mathrm{G}} = [0, 0, h_{\mathrm{G}}]$, and the 3D

positions of mobile device k and UAV u as $\boldsymbol{q}_k = [x_k, y_k, h_{\text{MD}}]$ and $\boldsymbol{q}_u = [x_u, y_u, h_u]$, respectively.

A. UAV-Enabled 3D Wireless Channel Model

We assume that the mobile devices can choose to connect to the GBS or the UAV for better channel quality in supporting 6G mURLLC. Define the binary variable $b_{k,u}$ ($k \in \{1, \ldots, K\}, u \in \{0, \ldots, U\}$) as follows:

$$b_{k,u} = \begin{cases} 1, & \text{if mobile user } k \text{ chooses to connect to UAV } u; \\ 0, & \text{otherwise,} \end{cases} \tag{1}$$

where $b_{k,0}$ represents the case where mobile user k chooses to connect to the GBS. Since each mobile user can only be associated to one UAV or the GBS, i.e.,

$$\sum_{u=0}^{U} b_{k,u} = 1. \tag{2}$$

1) Ground-to-Ground Channel Model: If mobile user k chooses to connect to the GBS, i.e., $b_{k,u} = 0$, then we consider the non-line-of-sight (NLoS) channels for the ground-to-ground channel model due to the obstacles between mobile devices and the GBS. We can ignore the LoS link due to the very small probability of LoS link. The channel propagation path loss, denoted by $PL_{k,\text{G}}$, in dB between mobile device k and the GBS can de derived as follows:

$$\begin{aligned} PL_{k,\text{G}} =& 13.54 + 39.08 \log_{10}(d_{k,\text{G}}) + 20 \log_{10}(f) \\ & - 0.6(h_{\text{MD}} - 1.5) \end{aligned} \tag{3}$$

where f is the carrier frequency, h_{MD} is the height of mobile devices, and $d_{k,\text{G}}$ is the distance between mobile device k and the GBS, which is given by

$$d_{k,\text{G}} = \|\boldsymbol{q}_k - \boldsymbol{q}_{\text{G}}\| \tag{4}$$

where $\|\cdot\|$ is the Euclidean distance. Then, we can derive the large-scale channel gain, denoted by $g_{k,\text{G}}$, between mobile device k and the GBS as follows:

$$g_{k,\text{G}} = 10^{-\frac{PL_{k,\text{G}}}{10}}. \tag{5}$$

Thus, we can derive the signal-to-noise ratio (SNR), denoted by $\gamma_{\text{G}}^{(l)}$, for transmitting the lth status update packet from mobile user k to the GBS as follows:

$$\gamma_{k,\text{G}}^{(l)} = \frac{\mathcal{P}_k 10^{-\frac{PL_{k,\text{G}}}{10}}}{(\sigma_{k,\text{G}})^2}, \quad l = 1, \ldots, N \tag{6}$$

where $\mathcal{P}_k$ denotes the transmit power at mobile user k and $\sigma_{k,\text{G}}^2$ is the noise power.

2) Ground-to-UAV 3D Channel Model: To guarantee that the UAV is located within the GBS's control area, we assume that the UAV is flying within an inverted cone centred at GBS with the largest radius of $D_{\max}$. We also assume that there is a small inverted cone centred at GBS with radius $D_{\min}$ ($D_{\max} > D_{\min}$) that the UAV will not fly into. Consider a 3D wireless channel model [23], which captures the fact that the LoS probability increases with elevation angle. In particular, the LoS probability, denoted by $P_{k,u}^{\text{LoS}}$, from mobile user k to UAV u can be derived as follows:

$$P_{k,u}^{\text{LoS}} = \frac{1}{1 + a \exp\left[-b(\alpha_{k,u} - a)\right]} \tag{7}$$

where $\alpha_{k,u}$ is the elevation angle between the mobile user k and UAV u and $a > 0$ and $b > 0$ are the constants that depend on the environment. Given the location of UAV u, we can derive the mean path loss, denoted by $PL_{k,u}$, in dB from mobile user k to UAV u as follows [23]:

$$PL_{k,u} = \frac{A}{1 + a \exp\left[-b(\alpha_{k,u} - a)\right]} + 20 \log_{10}(d_{k,u}) + C \tag{8}$$

where $d_{k,u}$ is the distance between mobile user k and UAV u, which is given as in the following equation:

$$d_{k,u} = \|\boldsymbol{q}_k - \boldsymbol{q}_u\| \tag{9}$$

and A and C are the constants, which are given by

$$\begin{cases} A = \eta_{\text{LoS}} - \eta_{\text{NLoS}}; \\ C = 20 \log_{10}\left(\frac{4\pi f_c}{c}\right) + \eta_{\text{NLoS}}, \end{cases} \tag{10}$$

where η_{LoS} and η_{NLoS} are the losses corresponding to the LoS and NLoS links, f_c is the carrier frequency in Hz, and c is the speed of light (m/s). Note that the channel between the mobile devices and the UAVs is mainly LoS propagation, i.e., $\eta_{\text{NLoS}} \gg \eta_{\text{LoS}}$ [23]. Then, the ground-to-UAV channel gain, denoted by $g_{k,u}$, from mobile user k to UAV u is given as follows:

$$g_{k,u} = 10^{-\frac{PL_{k,u}}{10}}. \tag{11}$$

We can then derive the SNR, denoted by $\gamma_{k,u}$, for transmitting the lth status update packet ($l = 1, \ldots, N$) from mobile user k to UAV u as follows:

$$\gamma_{k,u}^{(l)} = \frac{\mathcal{P}_k 10^{-\frac{C}{10}}}{(\sigma_{k,u} d_{k,u})^2} \exp\left\{\frac{-A(\log 10)}{10\left\{1 + a \exp\left[-b(\alpha_{k,u} - a)\right]\right\}}\right\} \tag{12}$$

where $\log(\cdot)$ represents $\log_e(\cdot)$, $\mathcal{P}_k$ denotes the transmit power at mobile user k, and $\sigma_{k,u}^2$ is the noise power.

B. Channel Coding Rate in the Finite Blocklength Regime

1) (n, M, ϵ)-code: We define a message set $\mathcal{M} = \{1, \ldots, M\}$ and a message m is uniformly distributed on $\mathcal{M}$, where M is the number of codewords. Correspondingly, we define a (n, M, ϵ)-code as follows:

- An encoder Υ: $\{1, \ldots, M\} \mapsto \mathbb{C}^n$ that maps the message $m \in \{1, \ldots, M\}$ into a codeword with length n, which is chosen randomly according to $\mathcal{N}(0, \overline{\mathcal{P}})$, where $\overline{\mathcal{P}}$ is the average transmit power.
- A decoder $\mathcal{D}$: $\mathbb{C}^n \mapsto \{1, \ldots, M\}$ that decodes the received message into $\widehat{m}$, where $\widehat{m}$ denotes the estimated received signal at the receiver. The decoder $\mathcal{D}$ needs to satisfy the following maximum error probability constraint:

$$\Pr\{\widehat{m} \neq m\} \leq \epsilon. \tag{13}$$

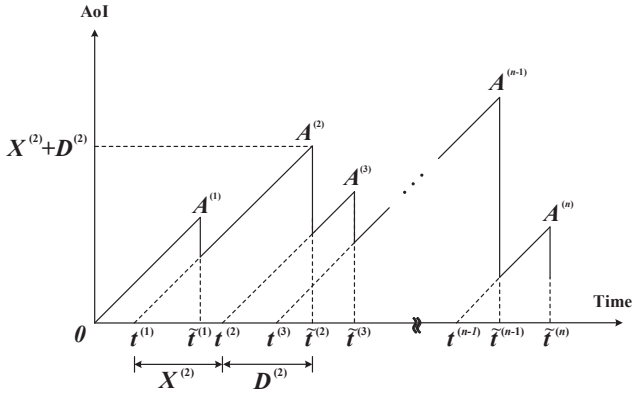

Fig. 2. AoI evolution as a function of time for N finite-blocklength status update packets.

2) Channel Coding Rate: Given a fixed channel coding rate $\log_2 M/n$, we can obtain the decoding error probability function, denoted by $\epsilon\left(\gamma_{k,u}^{(l)}\right)$, when transmitting the lth status update packet $(l = 1, \ldots, N)$ from mobile user k to UAV u as follows:

$$\epsilon\left(\gamma_{k,u}^{(l)}\right) \approx Q\left(\frac{C\left(\gamma_{k,u}^{(l)}\right) - \frac{\log_2 M}{n}}{\sqrt{V\left(\gamma_{k,u}^{(l)}\right)/n}}\right) \tag{14}$$

where $Q(\cdot)$ is the Q-function and $C\left(\gamma_{k,u}^{(l)}\right)$ and $V\left(\gamma_{k,u}^{(l)}\right)$ are the channel capacity and channel dispersion, respectively, from mobile user k to UAV u, which are given in the following equations:

$$\begin{cases} C\left(\gamma_{k,u}^{(l)}\right) = \log_2\left(1+\gamma_{k,u}^{(l)}\right); \\ V\left(\gamma_{k,u}^{(l)}\right) = 1 - \frac{1}{\left(1+\gamma_{k,u}^{(l)}\right)^2}. \end{cases} \tag{15}$$

III. UAV-Enabled AoI Violation Probability Analyses for 6G mURLLC in the Finite Blocklength Regime

A. AoI Metric Modelling

In order to measure and control the freshness of information, we adopt the concept of AoI, denoted by $a(t)$, as the performance metric at time instant t to describe the freshness of the decoded data at the receiver, which is given as follows:

$$a(t) = [t - \delta(t)]^+ \tag{16}$$

where $[x]^+ = \max\{0, x\}$ and $\delta(t)$ represents the time at which the most recently decoded packet is generated at the source node. Without loss of generality, we set $a(0) = 0$. As shown in Fig. 2, the source node generates finite-blocklength status update packets at time instants $t^{(1)}, t^{(2)}, \ldots, t^{(N)}$ and the finite-blocklength status update packets are successfully decoded at time instants $\tilde{t}^{(1)}, \tilde{t}^{(2)}, \ldots, \tilde{t}^{(N)}$. Observing form Fig. 2, we can derive the peak AoI, denoted by $A^{(l)}$, at time instant $t^{(l)}$ for transmitting the lth status update packet $(l = 1, \ldots, N)$ in the finite blocklength regime as follows:

$$A^{(l)} \triangleq A\left(t^{(l)}\right) = \tilde{t}^{(l)} - t^{(l-1)}. \tag{17}$$

Define $X^{(l)} \triangleq t^{(l)} - t^{(l-1)}$ as the interval between the arrival time of the $(l-1)$th status update packet and the lth status update packet and $D^{(l)} \triangleq \tilde{t}^{(l)} - t^{(l)}$ as the total system delay for transmitting the lth status update packet $(l = 1, \ldots, N)$. Then, the peak AoI $A^{(l)}$ at time instant $t^{(l)}$ for transmitting the lth status update packet in the finite blocklength regime can be rewritten as in the following equation:

$$A^{(l)} = X^{(l)} + D^{(l)}. \tag{18}$$

Assume that the processing delay and the propagation delay are negligible. Let

$$D^{(l)} = W^{(l)} + S^{(l)} \tag{19}$$

where $W^{(l)}$ is the waiting time in the queue for the lth status update packet and $S^{(l)}$ is the service time of the lth status update packet. Accordingly, for our proposed AoI-driven and UAV-enabled schemes, we can derive the peak AoI, denoted by $A_{k,u}^{(l)}$, for transmitting the lth status update packet from mobile user k to UAV u as in the following equation:

$$A_{k,u}^{(l)} \triangleq D_{k,u}^{(l)} + X_{k,u}^{(l)} \tag{20}$$

where $D_{k,u}^{(l)}$ is the total system delay for transmitting the lth status update packet from mobile user k to UAV u and $X_{k,u}^{(l)}$ is interval between the arrival time of the $(l-1)$th status update packet and the lth status update packet at mobile user k.

B. The Upper-Bounded Peak AoI Violation Probability for UAV-Enabled 6G mURLLC in the Finite Blocklength Regime

Denote by A_{th} the peak AoI threshold for our proposed AoI-driven and UAV-enabled scheme. We can derive the peak AoI violation probability, denoted by $\epsilon_{k,u}^{(l,\text{AoI})}$, for transmitting the lth status update packet $(l = 1, \ldots, N)$ from mobile user k to UAV u in the finite blocklength regime as follows:

$$\epsilon_{k,u}^{(l,\text{AoI})} \triangleq \Pr\left\{A_{k,u}^{(l)} > A_{\text{th}}\right\}. \tag{21}$$

Theorem 1: Given the peak AoI threshold A_{th}, an upper bound on the peak AoI violation probability $\epsilon_{k,u}^{(l,\text{AoI})}$ for our proposed AoI-driven and UAV-enabled scheme is given as follows:

$$\epsilon_{k,u}^{(l,\text{AoI})} \leq \frac{1}{A_{\text{th}}}\left\{\frac{\widetilde{\lambda}_{k,u}(nT)^2\left[1+\epsilon\left(\gamma_{k,u}^{(l)}\right)\right]}{2\left[1-\epsilon\left(\gamma_{k,u}^{(l)}\right)\right]^2\left[1-\frac{nT\widetilde{\lambda}_{k,u}}{1-\epsilon\left(\gamma_{k,u}^{(l)}\right)}\right]} + \frac{nT}{1-\epsilon\left(\gamma_{k,u}^{(l)}\right)} + \frac{1}{\widetilde{\lambda}_{k,u}}\right\}. \tag{22}$$

Proof: Using the Markov's inequality, we can derive an upper bound on the peak AoI violation probability $\epsilon_{k,u}^{(l,\text{AoI})}$ as follows:

$$\epsilon_{k,u}^{(l,\text{AoI})} \leq \frac{\mathbb{E}\left[A_{k,u}^{(l)}\right]}{A_{\text{th}}} = \frac{1}{A_{\text{th}}}\mathbb{E}\left[D_{k,u}^{(l)} + X_{k,u}^{(l)}\right] \tag{23}$$

where $\mathbb{E}[\cdot]$ is the expectation operation. Since $D_{k,u}^{(l)}$ and $X_{k,u}^{(l)}$ are independent with each other, we have

$$\epsilon_{k,u}^{(l,\text{AoI})} \leq \frac{1}{A_{\text{th}}}\left\{\mathbb{E}\left[D_{k,u}^{(l)}\right] + \mathbb{E}\left[X_{k,u}^{(l)}\right]\right\}. \tag{24}$$

We consider a FCFS queue and the arrivals of the packets follow a Poisson process with rate $\widetilde{\lambda}_{k,u}$ for mobile user k. We have

$$\mathbb{E}\left[X_{k,u}^{(l)}\right] = \frac{1}{\widetilde{\lambda}_{k,u}}. \tag{25}$$

Then, we assume that there is a reliable feedback between the mobile users and the UAVs [24]. Define T as the unit time for each channel use, i.e., the duration for each symbol. By applying the automatic repeat request (ARQ) protocol, we can derive the service time, denoted by $S_{k,u}^{(l)}$, in seconds for transmitting the lth status update packet $(l = 1, \ldots, N)$ from mobile user k to UAV u as follows:

$$S_{k,u}^{(l)} = nTL_{k,u} \tag{26}$$

where $L_{k,u}$ is the number of retransmissions using ARQ protocol. The probability density function (PDF) of the number of retransmissions $L_{k,u}$ follows the geometrically distribution with parameter $\epsilon\left(\gamma_{k,u}^{(l)}\right)$, which is given as follows:

$$P_{L_{k,u}}(\ell) = \left[1 - \epsilon\left(\gamma_{k,u}^{(l)}\right)\right]\left[\epsilon\left(\gamma_{k,u}^{(l)}\right)\right]^{\ell}. \tag{27}$$

Then, the average service time, denoted by $\mathbb{E}\left[S_{k,u}^{(l)}\right]$, is given as follows:

$$\mathbb{E}\left[S_{k,u}^{(l)}\right] = \frac{nT}{1 - \epsilon\left(\gamma_{k,u}^{(l)}\right)}. \tag{28}$$

We can also derive the expectation on $\left(S_{k,u}^{(l)}\right)^2$ as follows:

$$\mathbb{E}\left[\left(S_{k,u}^{(l)}\right)^2\right] = \frac{(nT)^2\left[1 + \epsilon\left(\gamma_{k,u}^{(l)}\right)\right]}{\left[1 - \epsilon\left(\gamma_{k,u}^{(l)}\right)\right]^2}. \tag{29}$$

Using the Pollaczek-Khinchin formula, we can derive the average system delay as follows:

$$\mathbb{E}\left[D_{k,u}^{(l)}\right] = \frac{\widetilde{\lambda}_{k,u}\mathbb{E}\left[\left(S_{k,u}^{(l)}\right)^2\right]}{2\left[1 - \widetilde{\lambda}_{k,u}\mathbb{E}\left[S_{k,u}^{(l)}\right]\right]} + \mathbb{E}\left[S_{k,u}^{(l)}\right]. \tag{30}$$

Then, by plugging Eqs. (25), (28), (29), and (30) into Eq. (24), we can obtain Eq. (22), which completes the proof of Theorem 1. ∎

IV. AoI-Driven Statistical Delay and Error-Rate Bounded QoS Provisioning in the Finite Blocklength Regime

A. The AoI-Driven ϵ-Effective Capacity in the Finite Blocklength Regime

Since both the peak AoI violation probability and decoding error probability are small enough, we have $\epsilon\left(\gamma_{k,u}^{(l)}\right)\epsilon_{k,u}^{(l,\text{AoI})} \to 0$. Thus, the overall error probability, denoted by $\epsilon_{k,u}^{(l,\text{o})}$, for both peak AoI violation and decoding error probabilities can be approximated as follows:

$$\epsilon_{k,u}^{(l,\text{o})} = \epsilon\left(\gamma_{k,u}^{(l)}\right) + \epsilon_{k,u}^{(l,\text{AoI})}. \tag{31}$$

Definition 1: For a (n, M, ϵ)-code, given a fixed channel coding rate $\log_2 M/n$, the AoI-driven ϵ-effective capacity, denoted by $EC_{k,u}^{(l)}(\theta_k)$, for transmitting the lth status update packet $(l = 1, \ldots, N)$ from mobile user k to UAV u in the finite blocklength regime is given as follows:

$$EC_{k,u}^{(l)}(\theta_k) \triangleq -\frac{1}{\theta_k}\log\left\{\mathbb{E}_\gamma\left[\epsilon_{k,u}^{(l,\text{o})} + \left(1 - \epsilon_{k,u}^{(l,\text{o})}\right)e^{-\theta_k \log_2 M}\right]\right\} \tag{32}$$

where $\mathbb{E}_\gamma[\cdot]$ denotes the expectation with respect to the value of the SNR and θ_k is defined as the *QoS exponent* for mobile device k. Then, using Eq. (22), we can derive an upper bound on the AoI-driven ϵ-effective capacity $EC_{k,u}^{(l)}(\theta_k)$ as follows:

$$\begin{aligned} EC_{k,u}^{(l)}(\theta_k) \leq -\frac{1}{\theta_k}\log\Bigg\{\mathbb{E}_\gamma\Bigg[\epsilon\left(\gamma_{k,u}^{(l)}\right) + \frac{1}{A_{\text{th}}}\Bigg\{\frac{\widetilde{\lambda}_{k,u}(nT)^2}{2} \\ \times \frac{\left[1 + \epsilon\left(\gamma_{k,u}^{(l)}\right)\right]}{\left[1 - \epsilon\left(\gamma_{k,u}^{(l)}\right)\right]^2\left[1 - \frac{nT\widetilde{\lambda}_{k,u}}{1 - \epsilon\left(\gamma_{k,u}^{(l)}\right)}\right]} + \frac{nT}{1 - \epsilon\left(\gamma_{k,u}^{(l)}\right)} + \frac{1}{\widetilde{\lambda}_{k,u}}\Bigg\} \\ + \Bigg\{1 - \epsilon\left(\gamma_{k,u}^{(l)}\right) - \frac{1}{A_{\text{th}}}\Bigg\{\frac{\widetilde{\lambda}_{k,u}(nT)^2\left[1 + \epsilon\left(\gamma_{k,u}^{(l)}\right)\right]}{2\left[1 - \epsilon\left(\gamma_{k,u}^{(l)}\right)\right]^2\left[1 - \frac{nT\widetilde{\lambda}_{k,u}}{1 - \epsilon\left(\gamma_{k,u}^{(l)}\right)}\right]} \\ + \frac{nT}{1 - \epsilon\left(\gamma_{k,u}^{(l)}\right)} + \frac{1}{\widetilde{\lambda}_{k,u}}\Bigg\}e^{-\theta_k \log_2 M}\Bigg\}\Bigg]\Bigg\}. \end{aligned} \tag{33}$$

B. AoI-Driven ϵ-Effective Capacity Maximization Under Peak AoI Violation Probability Constraint Using FBC

Denote by $\boldsymbol{\mathcal{P}} = [\mathcal{P}_1, \ldots, \mathcal{P}_K]$ and $\boldsymbol{b} = [b_{1,1}, b_{1,2}, \ldots, b_{K,U}]$ the transmit power vector and user association vector for all K mobile users, respectively. Considering the peak AoI violation probability constraint, we can formulate the optimization problem $\mathbf{P_1}$ to maximize the aggregate AoI-driven ϵ-effective capacity $EC_{k,u}^{(l)}(\theta_k)$ for our proposed AoI-driven and UAV-enabled schemes in the finite blocklength regime as follows:

$$\mathbf{P_1}: \arg\max_{\{\boldsymbol{\mathcal{P}}, \boldsymbol{b}, \boldsymbol{q}_u\}}\left\{\sum_{k=1}^{K} b_{k,u} EC_{k,u}^{(l)}(\theta_k)\right\} \tag{34}$$

$$\text{s.t. } C1: \sum_{u=0}^{U} b_{k,u} = 1, \quad \forall k; \tag{35}$$

$$C2: \epsilon\left(\gamma_{k,u}^{(l)}\right) \leq \epsilon_{\text{th}}, \quad \forall k; \tag{36}$$

$$C3: \mathbb{E}\left[\mathcal{P}_k\right] \leq \overline{\mathcal{P}}, \quad \forall k; \tag{37}$$

$$C4: D_{\min} \leq x_u \leq D_{\max}, \quad \forall u; \tag{38}$$

$$C5: D_{\min} \leq y_u \leq D_{\max}, \quad \forall u, \tag{39}$$

where ϵ_{th} is the upper bound on the decoding error probability. However, the coupling of different optimization variables $\{\boldsymbol{\mathcal{P}}, \boldsymbol{b}, \boldsymbol{q}_u\}$ makes $\mathbf{P_1}$ a non-convex optimization problem. Therefore, we cannot directly solve $\mathbf{P_1}$ by using the standard convex optimization techniques. To solve the maximization problem $\mathbf{P_1}$, we can devide $\mathbf{P_1}$ is into the following two sub-problems.

1) Optimal User Association and Power Allocation Policy: Given the 3D location $\boldsymbol{q}_u$ of UAV u, we need to find the optimal user association and power allocation policies for each mobile device to maximize the aggregate AoI-driven ϵ-effective capacity. We can convert the optimization problem $\mathbf{P_1}$ in Eq. (34) into the following suboptimal problem $\mathbf{P_2}$:

$$\mathbf{P_2}: \arg\max_{\{\boldsymbol{\mathcal{P}}, \boldsymbol{b}\}} \left\{ \sum_{k=1}^{K} b_{k,u} E C_{k,u}^{(l)}(\theta_k) \right\} \tag{40}$$

subject to the constraints $C1$, $C2$, and $C3$ given in Eqs. (35), (36), and (37), respectively. However, the objective function in $\mathbf{P_2}$ given by Eq. (40) is still non-concave. We can then convert $\mathbf{P_2}$ into an equivalent minimization problem $\mathbf{P_3}$ as follows:

$$\mathbf{P_3}: \arg\min_{\{\boldsymbol{\mathcal{P}}, \boldsymbol{b}\}} \left\{ \sum_{k=1}^{K} b_{k,u} \mathbb{E}_\gamma \left[\epsilon_{k,u}^{(l,\text{o})} + \left(1 - \epsilon_{k,u}^{(l,\text{o})}\right) e^{-\theta_k \log_2 M} \right] \right\} \tag{41}$$

subject to the constraints $C1$, $C2$, and $C3$ given in Eqs. (35), (36), and (37), respectively. However, the constraint $C2$ in Eq. (36) is non-convex. To convert the non-convex constraint $C2$ into a convex set, first we need to analyze the monotonicity of the decoding error probability function with respect to the SNR as detailed in the following lemma.

Lemma 1: The decoding error probability function $\epsilon\left(\gamma_{k,u}^{(l)}\right)$ is *monotonically decreasing* with respect to the SNR $\gamma_{k,u}^{(l)}$.

Proof: Due to the space limitation, we omit the proof of Lemma 1 in this paper. ∎

Then, we define the following auxiliary function:

$$\Phi\left(\gamma_{k,u}^{(l)}\right) \triangleq \epsilon\left(\gamma_{k,u}^{(l)}\right). \tag{42}$$

Using the result in Lemma 1, we obtain that the function $\Phi\left(\gamma_{k,u}^{(l)}\right)$ is decreasing with respect to the SNR $\gamma_{k,u}^{(l)}$. We can convert the inequality in constraint $C2$ given by Eq. (36) into an equivalent constraint $C2'$ as follows:

$$C2': \gamma_{k,u}^{(l)} \geq \Phi^{-1}\left(\epsilon_{\text{th}}\right) \tag{43}$$

where $\Phi^{-1}(\cdot)$ is the inverse of the function $\Phi\left(\gamma_{k,u}^{(l)}\right)$ given in Eq. (42). Using Eqs. (12) and (43), we have

$$C2': \mathcal{P}_k \leq \frac{(\sigma_{k,u} d_{k,u})^2 \Phi^{-1}\left(\epsilon_{\text{th}}\right)}{10^{-\frac{C}{10}} \exp\left\{ \frac{-A(\log 10)}{10[1 + a\exp[-b(\alpha_{k,u} - a)]]} \right\}}, \quad \forall k. \tag{44}$$

We can obtain that the constraint $C2'$ is convex. Furthermore, we need to characterize the convexity of $\mathbf{P_3}$ with respect to the transmit power $\boldsymbol{\mathcal{P}}$. Since the SNR is a linear function of the transmit power, it is equivalent to analyze the convexity of $\mathbf{P_3}$ with respect to the SNR. Using Eq. (41), we define the following function:

$$\widetilde{F}\left(\gamma_{k,u}^{(l)}\right) \triangleq \mathbb{E}_\gamma \Bigg[\epsilon\left(\gamma_{k,u}^{(l)}\right) + \epsilon_{k,u}^{(l,\text{AoI})} + \left[1 - \epsilon\left(\gamma_{k,u}^{(l)}\right) - \epsilon_{k,u}^{(l,\text{AoI})}\right] \times e^{-\theta_k \log_2 M} \Bigg] \tag{45}$$

Since we have shown that the decoding error probability function $\epsilon\left(\gamma_{k,u}^{(l)}\right)$ is decreasing with respect to the SNR, by taking the second-order derivative of the function $\widetilde{F}\left(\gamma_{k,u}^{(l)}\right)$ with respect to the SNR, we can obtain

$$\frac{\partial^2 \widetilde{F}\left(\gamma_{k,u}^{(l)}\right)}{\partial\left(\gamma_{k,u}^{(l)}\right)^2} = \mathbb{E}_\gamma \left[\frac{\partial^2 \epsilon_{k,u}^{(l,\text{AoI})}}{\partial\left(\gamma_{k,u}^{(l)}\right)^2} \left(1 - e^{-\theta_k \log_2 M}\right) \right] \tag{46}$$

We have $1 - e^{-\theta_k \log_2 M} > 0$ for $\theta_k > 0$. As a result, to characterize the convexity of $\mathbf{P_3}$, it is equivalent to analyze the convexity of the peak AoI violation probability function with respect to the SNR $\gamma_{k,u}^{(l)}$, which motivates the theorem that follows.

Theorem 2: **If** the decoding error probability $\epsilon\left(\gamma_{k,u}^{(l)}\right)$ is specified by Eq. (14) and the upper bounded peak AoI violation probability is specified by Eq. (22), **then** the peak AoI violation probability $\epsilon_{k,u}^{(l,\text{AoI})}$ given by Eq. (22) is a *strictly convex* function with respect to the SNR $\gamma_{k,u}^{(l)}$ if the following condition holds:

$$n < \frac{1 - \epsilon\left(\gamma_{k,u}^{(l)}\right)}{T\widetilde{\lambda}_{k,u}} \tag{47}$$

where $\epsilon\left(\gamma_{k,u}^{(l)}\right)$ is the decoding error probability given by Eq. (14).

Proof: To analyze the convexity of the peak AoI violation probability function with respect to the SNR, we need to proceed with the following steps. First, we define the following auxiliary function:

$$F\left(\gamma_{k,u}^{(l)}\right) \triangleq \frac{\widetilde{\lambda}_{k,u}(nT)^2 \left[1 + \epsilon\left(\gamma_{k,u}^{(l)}\right)\right]}{2\left[1 - \epsilon\left(\gamma_{k,u}^{(l)}\right)\right]^2 \left[1 - \frac{nT\widetilde{\lambda}_{k,u}}{1 - \epsilon\left(\gamma_{k,u}^{(l)}\right)}\right]} + \frac{nT}{1 - \epsilon\left(\gamma_{k,u}^{(l)}\right)} + \frac{1}{\widetilde{\lambda}_{k,u}}. \tag{48}$$

Thus, we have

$$\epsilon_{k,u}^{(l,\text{AoI})} \approx \frac{1}{A_{\text{th}}} \left[F\left(\gamma_{k,u}^{(l)}\right) \right]. \tag{49}$$

Second, we take the first-order derivative of the function $F\left(\gamma_{k,u}^{(l)}\right)$ with respect to the SNR $\gamma_{k,u}^{(l)}$ as follows:

$$\begin{aligned}\frac{\partial F\left(\gamma_{k,u}^{(l)}\right)}{\partial \gamma_{k,u}^{(l)}} =& \frac{\widetilde{\lambda}_{k,u}(nT)^2}{2}\Bigg\{\frac{\partial \epsilon\left(\gamma_{k,u}^{(l)}\right)}{\partial \gamma_{k,u}^{(l)}}\left[1-\epsilon\left(\gamma_{k,u}^{(l)}\right)\right] \\ &\times\left[1-\epsilon\left(\gamma_{k,u}^{(l)}\right)-nT\widetilde{\lambda}_{k,u}\right]+\left[1+\epsilon\left(\gamma_{k,u}^{(l)}\right)\right] \\ &\times\Bigg\{\frac{\partial \epsilon\left(\gamma_{k,u}^{(l)}\right)}{\partial \gamma_{k,u}^{(l)}}\left[1-\epsilon\left(\gamma_{k,u}^{(l)}\right)-nT\widetilde{\lambda}_{k,u}\right] \\ &+\frac{\partial \epsilon\left(\gamma_{k,u}^{(l)}\right)}{\partial \gamma_{k,u}^{(l)}}\left[1-\epsilon\left(\gamma_{k,u}^{(l)}\right)\right]\Bigg\}\Bigg\}\Bigg\{\left[1-\epsilon\left(\gamma_{k,u}^{(l)}\right)\right] \\ &\times\left[1-\epsilon\left(\gamma_{k,u}^{(l)}\right)-nT\widetilde{\lambda}_{k,u}\right]\Bigg\}^{-2} \\ &+\frac{nT}{\left[1-\epsilon\left(\gamma_{k,u}^{(l)}\right)\right]^2}\frac{\partial \epsilon\left(\gamma_{k,u}^{(l)}\right)}{\partial \gamma_{k,u}^{(l)}} \\ =& \frac{\widetilde{\lambda}_{k,u}(nT)^2}{2}\Bigg\{2\left[1-\epsilon\left(\gamma_{k,u}^{(l)}\right)-nT\widetilde{\lambda}_{k,u}\right]\frac{\partial \epsilon\left(\gamma_{k,u}^{(l)}\right)}{\partial \gamma_{k,u}^{(l)}} \\ &+\left\{1-\left[\epsilon\left(\gamma_{k,u}^{(l)}\right)\right]^2\right\}\frac{\partial \epsilon\left(\gamma_{k,u}^{(l)}\right)}{\partial \gamma_{k,u}^{(l)}}\Bigg\} \\ &\times\left\{\left[1-\epsilon\left(\gamma_{k,u}^{(l)}\right)\right]\left[1-\epsilon\left(\gamma_{k,u}^{(l)}\right)-nT\widetilde{\lambda}_{k,u}\right]\right\}^{-2} \\ &+\frac{nT}{\left[1-\epsilon\left(\gamma_{k,u}^{(l)}\right)\right]^2}\frac{\partial \epsilon\left(\gamma_{k,u}^{(l)}\right)}{\partial \gamma_{k,u}^{(l)}}. \end{aligned} \tag{50}$$

Third, based on Eq. (50), we take the second-order derivative of the function $F\left(\gamma_{k,u}^{(l)}\right)$ with respect to the SNR $\gamma_{k,u}^{(l)}$ as follows:

$$\begin{aligned}&\frac{\partial^2 F\left(\gamma_{k,u}^{(l)}\right)}{\partial\left(\gamma_{k,u}^{(l)}\right)^2} \\ &= \frac{\widetilde{\lambda}_{k,u}(nT)^2}{2}\Bigg\{\Bigg[\frac{\partial^2 \epsilon\left(\gamma_{k,u}^{(l)}\right)}{\partial\left(\gamma_{k,u}^{(l)}\right)^2}2\left[1-\epsilon\left(\gamma_{k,u}^{(l)}\right)-nT\widetilde{\lambda}_{k,u}\right] \\ &\quad-2\left[1+\epsilon\left(\gamma_{k,u}^{(l)}\right)\right]\left[\frac{\partial \epsilon\left(\gamma_{k,u}^{(l)}\right)}{\partial \gamma_{k,u}^{(l)}}\right]^2+\left\{1-\left[\epsilon\left(\gamma_{k,u}^{(l)}\right)^2\right]\right\} \\ &\quad\times\frac{\partial^2 \epsilon\left(\gamma_{k,u}^{(l)}\right)}{\partial\left(\gamma_{k,u}^{(l)}\right)^2}\Bigg]\Bigg\{\left[1-\epsilon\left(\gamma_{k,u}^{(l)}\right)\right]\left[1-\epsilon\left(\gamma_{k,u}^{(l)}\right)-nT\widetilde{\lambda}_{k,u}\right]\Bigg\}^2 \\ &\quad+\Bigg\{2\left[1-\epsilon\left(\gamma_{k,u}^{(l)}\right)-nT\widetilde{\lambda}_{k,u}\right]\frac{\partial \epsilon\left(\gamma_{k,u}^{(l)}\right)}{\partial \gamma_{k,u}^{(l)}} \\ &\quad+\left\{1-\left[\epsilon\left(\gamma_{k,u}^{(l)}\right)\right]^2\right\}\frac{\partial \epsilon\left(\gamma_{k,u}^{(l)}\right)}{\partial \gamma_{k,u}^{(l)}}\Bigg\}\Bigg\{2\left[1-\epsilon\left(\gamma_{k,u}^{(l)}\right)\right] \\ &\quad\times\left[1-\epsilon\left(\gamma_{k,u}^{(l)}\right)-nT\widetilde{\lambda}_{k,u}\right]\Bigg\}\Bigg\{\left[1-\epsilon\left(\gamma_{k,u}^{(l)}\right)-nT\widetilde{\lambda}_{k,u}\right] \\ &\quad\times\frac{\partial \epsilon\left(\gamma_{k,u}^{(l)}\right)}{\partial \gamma_{k,u}^{(l)}}+\left[1-\epsilon\left(\gamma_{k,u}^{(l)}\right)\right]\frac{\partial \epsilon\left(\gamma_{k,u}^{(l)}\right)}{\partial \gamma_{k,u}^{(l)}}\Bigg\}\Bigg\} \\ &\quad\times\Bigg\{\left[1-\epsilon\left(\gamma_{k,u}^{(l)}\right)\right]\left[1-\epsilon\left(\gamma_{k,u}^{(l)}\right)-nT\widetilde{\lambda}_{k,u}\right]\Bigg\}^{-4} \\ &\quad+\frac{nT}{\left[1-\epsilon\left(\gamma_{k,u}^{(l)}\right)\right]^4}\Bigg\{\left[1-\epsilon\left(\gamma_{k,u}^{(l)}\right)\right]^2\frac{\partial^2 \epsilon\left(\gamma_{k,u}^{(l)}\right)}{\partial\left(\gamma_{k,u}^{(l)}\right)^2} \\ &\quad+2\left[1-\epsilon\left(\gamma_{k,u}^{(l)}\right)\right]\left[\frac{\partial \epsilon\left(\gamma_{k,u}^{(l)}\right)}{\partial \gamma_{k,u}^{(l)}}\right]^2\Bigg\} \\ &= \frac{\widetilde{\lambda}_{k,u}(nT)^2}{2}\left[1-\epsilon\left(\gamma_{k,u}^{(l)}\right)\right]\left[1-\epsilon\left(\gamma_{k,u}^{(l)}\right)-nT\widetilde{\lambda}_{k,u}\right] \\ &\quad\times\Bigg\{\frac{\partial^2 \epsilon\left(\gamma_{k,u}^{(l)}\right)}{\partial\left(\gamma_{k,u}^{(l)}\right)^2}2\left[1-\epsilon\left(\gamma_{k,u}^{(l)}\right)-nT\widetilde{\lambda}_{k,u}\right]^2\left[1-\epsilon\left(\gamma_{k,u}^{(l)}\right)\right] \\ &\quad+\left\{1-\left[\epsilon\left(\gamma_{k,u}^{(l)}\right)^2\right]\right\}\frac{\partial^2 \epsilon\left(\gamma_{k,u}^{(l)}\right)}{\partial\left(\gamma_{k,u}^{(l)}\right)^2}\left[1-\epsilon\left(\gamma_{k,u}^{(l)}\right)\right] \\ &\quad\times\left[1-\epsilon\left(\gamma_{k,u}^{(l)}\right)-nT\widetilde{\lambda}_{k,u}\right] \\ &\quad+4\left[1-\epsilon\left(\gamma_{k,u}^{(l)}\right)-nT\widetilde{\lambda}_{k,u}\right]^2\left[\frac{\partial \epsilon\left(\gamma_{k,u}^{(l)}\right)}{\partial \gamma_{k,u}^{(l)}}\right]^2 \\ &\quad+2\left[1-3\epsilon\left(\gamma_{k,u}^{(l)}\right)\right]\left[1-\epsilon\left(\gamma_{k,u}^{(l)}\right)-nT\widetilde{\lambda}_{k,u}\right]\left[\frac{\partial \epsilon\left(\gamma_{k,u}^{(l)}\right)}{\partial \gamma_{k,u}^{(l)}}\right]^2 \\ &\quad+2\left[1+\epsilon\left(\gamma_{k,u}^{(l)}\right)\right]\left[1-\epsilon\left(\gamma_{k,u}^{(l)}\right)-nT\widetilde{\lambda}_{k,u}\right]\left[\frac{\partial \epsilon\left(\gamma_{k,u}^{(l)}\right)}{\partial \gamma_{k,u}^{(l)}}\right]^2 \\ &\quad+2\left\{1-\left[\epsilon\left(\gamma_{k,u}^{(l)}\right)\right]^2\right\}\left[1-\epsilon\left(\gamma_{k,u}^{(l)}\right)\right]\left[\frac{\partial \epsilon\left(\gamma_{k,u}^{(l)}\right)}{\partial \gamma_{k,u}^{(l)}}\right]^2\Bigg\} \\ &\quad\times\Bigg\{\left[1-\epsilon\left(\gamma_{k,u}^{(l)}\right)\right]\left[1-\epsilon\left(\gamma_{k,u}^{(l)}\right)-nT\widetilde{\lambda}_{k,u}\right]\Bigg\}^{-4} \\ &\quad+\frac{nT}{\left[1-\epsilon\left(\gamma_{k,u}^{(l)}\right)\right]^4}\Bigg\{\left[1-\epsilon\left(\gamma_{k,u}^{(l)}\right)\right]^2\frac{\partial^2 \epsilon\left(\gamma_{k,u}^{(l)}\right)}{\partial\left(\gamma_{k,u}^{(l)}\right)^2} \\ &\quad+2\left[1-\epsilon\left(\gamma_{k,u}^{(l)}\right)\right]\left[\frac{\partial \epsilon\left(\gamma_{k,u}^{(l)}\right)}{\partial \gamma_{k,u}^{(l)}}\right]^2\Bigg\}. \end{aligned} \tag{51}$$

Observing Eq. (51), we can obtain

$$\frac{\partial^2 F\left(\gamma_{k,u}^{(l)}\right)}{\partial\left(\gamma_{k,u}^{(l)}\right)^2} > 0, \tag{52}$$

if the inequation given in Eq. (47) holds. Therefore, combining Eqs. (49) and (52), we obtain that the peak AoI violation probability function $\epsilon_{k,u}^{(l,\text{AoI})}$ is convex with respect to the SNR if Eq. (47) holds, thus completing the proof of Theorem 2. ■

Theorem 2 implies that the objective function of the minimization problem $\mathbf{P_3}$ in Eq. (41) is convex in $\boldsymbol{\mathcal{P}}$ subject to the constraints constraints $C1$, $C2'$, and $C3$ specified by Eqs. (35), (44), and (37). Thus, the minimization problem $\mathbf{P_3}$ can be considered as a mixed integer disciplined convex program (MIDCP) [25]. We can efficiently find the optimal solution to $\mathbf{P_3}$ by applying the combination of a traditional convex optimization algorithm with an exhaustive search method.

2) Optimal UAV Trajectory Policy: Once the optimal user association is selected in the precious step, the maximization problem $\mathbf{P_1}$ becomes a feasibility optimization problem in $\boldsymbol{q}_u$. Therefore, we need to find the optimal UAV trajectory policy to maximize aggregate AoI-driven ϵ-effective capacity. We can convert the maximization problem $\mathbf{P_1}$ into the following suboptimal problem $\mathbf{P_4}$:

$$\mathbf{P_4}: \arg \min_{\{\boldsymbol{\mathcal{P}}, \boldsymbol{q}_u\}} \left\{ \sum_{k=1}^{K} \mathbb{E}_\gamma \left[\epsilon_{k,u}^{(l,\text{o})} + \left(1 - \epsilon_{k,u}^{(l,\text{o})}\right) e^{-\theta_k \log_2 M} \right] \right\} \tag{53}$$

subject to the constraints $C2'$, $C4$, and $C5$ given in Eqs. (44), (38), and (39). Since $d_{k,u} = \|\boldsymbol{q}_k - \boldsymbol{q}_u\|$, we can easily show that the constraint $C2'$ is convex with respect to $\boldsymbol{q}_u$. In addition, we can show that the objective function in $\mathbf{P_4}$ is convex with respect to $\|\boldsymbol{q}_k - \boldsymbol{q}_u\|^2$. As a result, the objective function in $\mathbf{P_4}$ can be quickly and efficiently solved by applying the exhaustive search method, such as branch and bound algorithm with appropriate pre-specified limits.

As a result, we can solve the optimization problem $\mathbf{P_1}$ given by Eq. (34) in an iterative manner until it converges to a pre-specified accuracy. We define $\boldsymbol{\mathcal{P}}^{(j)}$, $\boldsymbol{b}^{(j)}$, and $\boldsymbol{q}_u^{(j)}$ as the transmit power vector, user association vector, and 3D UAV location vector in the jth iteration, respectively. Define τ as the iteration tolerance. We develop the iterative algorithm as shown in **Algorithm 1** to solve $\mathbf{P_1}$ for our proposed statistical delay and error-rate bounded QoS provisioning in supporting 6G mURLLC over AoI-driven and UAV-enabled wireless networks.

V. Performance Evaluations

We use MATLAB-based simulations to validate and evaluate our proposed 6G mURLLC-enabled AoI-driven and UAV-enabled wireless networks under statistical delay and error-rate bounded QoS provisioning in the finite blocklength regime. Throughout our simulations, we set the packet size of each status update information $M \in [300, 800]$ bits, the unit time for each channel use $T = \frac{1}{M}$, the blocklength $n \in [100, 600]$,

Algorithm 1 : Iterative algorithm for solving $\mathbf{P_1}$ in Eq.(34)

Input: $K, U, D_{\max}, D_{\min}, \epsilon_{th}, \boldsymbol{q}_k, n, M, T, \widetilde{\lambda}_{k,u}, \overline{\mathcal{P}}$ and a iteration tolerance τ
Initialization: $j = 0$ and $\left\{\boldsymbol{\mathcal{P}}^{(0)}, \boldsymbol{b}^{(0)}, \boldsymbol{q}_u^{(0)}\right\}$
Repeat
Step 1:
Given $\boldsymbol{q}_u^{(j)}$, calculate $\boldsymbol{\mathcal{P}}^{(j)}$ and $\boldsymbol{b}^{(j)}$ by solving $\mathbf{P_3}$ in Eq. (41)
Step 2:
Given $\boldsymbol{\mathcal{P}}^{(j)}$ and $\boldsymbol{b}^{(j)}$, calculate $\boldsymbol{q}_u^{(j+1)}$ to solve $\mathbf{P_4}$ in Eq. (53)
$j \leftarrow (j+1)$
Until $\frac{\boldsymbol{q}_u^{(j)} - \boldsymbol{q}_u^{(j-1)}}{\boldsymbol{q}_u^{(j)}} \leq \tau$

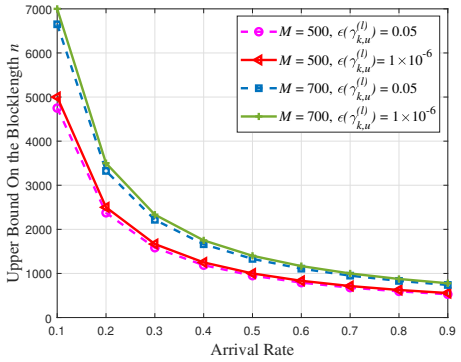

Fig. 3. The upper bound on the blocklength n vs. arrival rate $\widetilde{\lambda}_{k,u}$ for our proposed AoI-driven and UAV-enabled scheme using FBC.

the number of mobile users $K = 200$, the altitude of mobile devices $h_{\text{MU}} = 1.5$ m, the altitude of UAVs $h_u = 100$ m.

Using Eq. (47), Fig. 3 plots the upper bound on the blocklength n with different arrival rates $\widetilde{\lambda}_{k,u}$ in status updates/unit time. As shown in Fig. 3, the upper bound on the blocklength n decreases as the arrival rate $\widetilde{\lambda}_{k,u}$ increases. Fig. 3 also shows that the decoding error probability has only a small impact on the upper bound of the blocklength n. We can observe from Fig. 3 that setting $M = 500$ bits and $\epsilon\left(\gamma_{k,u}^{(l)}\right) = 1 \times 10^{-6}$, the upper bound on the blocklength n decreases from 5000 to 556 as the arrival rate $\widetilde{\lambda}_{k,u}$ increases from 0.1 to 0.9 using Eq. (47). Since the blocklength n for the time-sensitive status update information is normally very small, i.e., Eq. (47) holds in most cases, the convexity of the peak AoI violation probability function in Theorem 2 is generally true for our proposed AoI-driven and UAV-enabled schemes.

Setting the SNR $\gamma_{k,u}^{(l)} = 5$ dB and blocklength $n = 300$, Fig. 4 depicts the peak AoI as a function of the arrival rate $\widetilde{\lambda}_{k,u}$ as compared with the FCFS scheme without packet management [26]. Fig. 4 shows that the peak AoI first decreases as the arrival rate increases to a certain point, then it starts to increase as the arrival rate increases. Given a packet size M, there exists an optimal point that minimizes the peak AoI and the peak AoI increases significantly when the arrival rate deviates from the optimal point. This implies that the queue stability can be easily achieved when the arrival rate is low. When the arrival rate increases, data packets within the queue

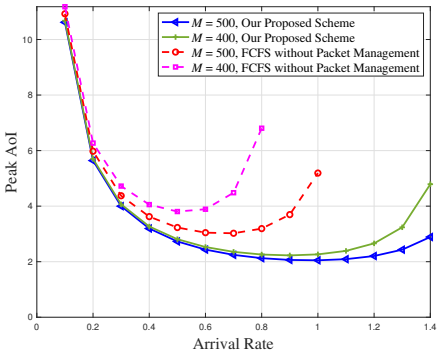

Fig. 4. The peak AoI vs. arrival rate $\widetilde{\lambda}_{k,u}$ for our proposed AoI-driven and UAV-enabled scheme in the finite blocklength regime.

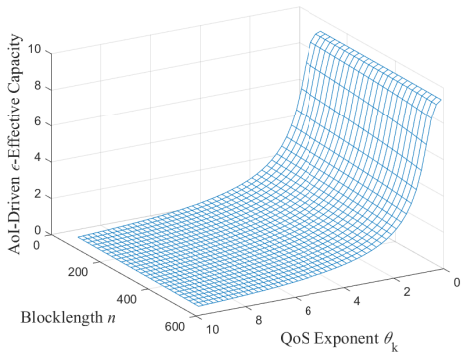

Fig. 6. The AoI-driven ϵ-effective capacity vs. blocklength n and QoS exponent θ_k for our proposed AoI-driven and UAV-enabled scheme using FBC.

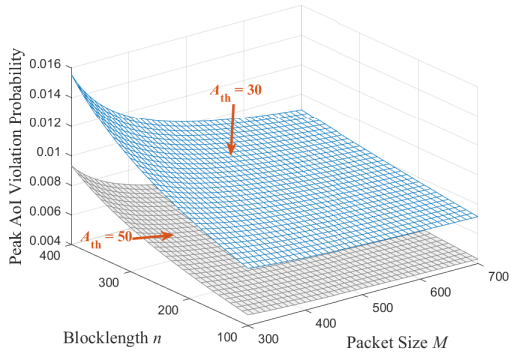

Fig. 5. The peak AoI violation probability function $\epsilon_{k,u}^{(l,\mathrm{AoI})}$ vs. blocklength n and packet size M for our proposed scheme using FBC.

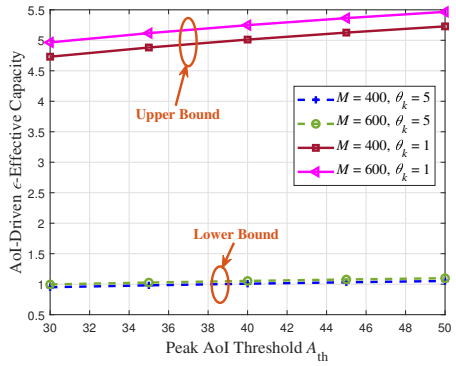

Fig. 7. The AoI-driven ϵ-effective capacity vs. peak AoI threshold A_{th} for our proposed AoI-driven and UAV-enabled scheme using FBC.

are transmitted more frequently to maintain the queue stability, achieving a lower value of peak AoI. When the arrival rate is too large, it is difficult to stabilize the queues. This will cause the queue to build up, which leads to the increased value of the peak AoI. Fig. 4 also shows that our proposed schemes outperform the FCFS scheme without packet management in terms of the peak AoI for a large range of arrival rate.

We set the SNR $\gamma_{k,u}^{(l)} = 5$ dB, the arrival rate $\widetilde{\lambda}_{k,u} = 0.7$, and the peak AoI threshold $A_{\mathrm{th}} = \{30, 50\}$ ms. Fig. 5 depicts the peak AoI violation probability $\epsilon_{k,u}^{(l,\mathrm{AoI})}$ as a function of both blocklength n and status update packet size M using FBC. Fig. 5 shows that the peak AoI violation probability $\epsilon_{k,u}^{(l,\mathrm{AoI})}$ increases with the blocklength n and decreases with the packet size M, respectively.

Setting the status update packet size $M = 700$ bits, Fig. 6 plots the AoI-driven ϵ-effective capacity with varying blocklengths n and QoS exponents θ_k. Fig. 6 shows that when the QoS exponent θ_k becomes more stringent, i.e., $\theta_k \to \infty$, the AoI-driven ϵ-effective capacity goes to zero. In addition, setting the blocklength $n = 300$ and the QoS exponent $\theta_k \in \{1, 5\}$, Fig. 7 depicts the AoI-driven ϵ-effective capacity as a function of the peak AoI threshold A_{th}. As shown in Fig. 7, the AoI-driven ϵ-effective capacity is an increasing function of the peak AoI threshold A_{th}, which implies that when the peak AoI threshold A_{th} is loose, i.e., A_{th} is large, we can achieve a larger value of the AoI-driven ϵ-effective capacity. We can observe from Fig. 6 and Fig. 7 that a smaller QoS exponent $\theta_k \to 0$ and a larger QoS exponent $\theta_k \to \infty$ set an upper bound and lower bound on the AoI-driven ϵ-effective capacity, respectively.

VI. Conclusions

We have proposed the AoI-driven statistical delay and error-rate bounded QoS provisioning schemes to efficiently support mURLLC over UAV-enabled 6G wireless networks in the finite blocklength regime. In particular, we have developed the UAV-enabled wireless networking models with 3D wireless channel and the channel coding rate model using FBC. Then, we have built up the AoI-metric based modeling frameworks in the finite blocklength regime. Taking into account the peak AoI violation probability, we have formulated and solved the AoI-driven ϵ-effective capacity maximization problems in supporting statistical delay and error-rate bounded QoS provisioning. We have conducted the extensive simulations to validate and evaluate our developed schemes to support statistical delay and error-rate bounded QoS provisioning.

REFERENCES

[1] X. Zhang, J. Tang, H.-H. Chen, S. Ci, and M. Guizani, "Cross-layer-based modeling for quality of service guarantees in mobile wireless networks," *IEEE Communications Magazine*, vol. 44, no. 1, pp. 100–106, 2006.

[2] J. Tang and X. Zhang, "Quality-of-service driven power and rate adaptation over wireless links," *IEEE Transactions on Wireless Communications*, vol. 6, no. 8, pp. 3058–3068, 2007.

[3] J. Tang and X. Zhang, "Cross-layer resource allocation over wireless relay networks for quality of service provisioning," *IEEE Journal on Selected Areas in Communications*, vol. 25, no. 4, pp. 645–656, May 2007.

[4] H. Su and X. Zhang, "Cross-layer based opportunistic MAC protocols for QoS provisionings over cognitive radio wireless networks," *IEEE Journal on Selected Areas in Communications*, vol. 26, no. 1, pp. 118–129, Jan. 2008.

[5] W. Cheng, X. Zhang, and H. Zhang, "Heterogeneous statistical QoS provisioning for downlink transmissions over mobile wireless cellular networks," in *Proceedings of IEEE GLOBECOM 2014*, 2014, pp. 4757–4763.

[6] X. Zhang, W. Cheng, and H. Zhang, "Heterogeneous statistical QoS provisioning over 5G mobile wireless networks," *IEEE Network Magazine*, vol. 28, no. 6, pp. 46–53, Nov. 2014.

[7] H. Ji, S. Park, J. Yeo, Y. Kim, J. Lee, and B. Shim, "Ultra-reliable and low-latency communications in 5G downlink: physical layer aspects," *IEEE Wireless Communications*, vol. 25, no. 3, pp. 124–130, June 2018.

[8] P. Mary, J. Gorce, A. Unsal, and H. V. Poor, "Finite blocklength information theory: what is the practical impact on wireless communications?" in *Proceedings of IEEE Globecom Workshops*, 2016, pp. 1–6.

[9] Y. Polyanskiy, H. V. Poor, and S. Verdú, "Channel coding rate in the finite blocklength regime," *IEEE Transactions on Information Theory*, vol. 56, no. 5, pp. 2307–2359, May 2010.

[10] Y. Polyanskiy and S. Verdú, "Empirical distribution of good channel codes with non-vanishing error probability," *IEEE Transactions on Information Theory*, vol. 60, no. 1, pp. 5–21, 2013.

[11] C. She, C. Liu, T. Q. S. Quek, C. Yang, and Y. Li, "UAV-assisted uplink transmission for ultra-reliable and low-latency communications," in *Proceedings of 2018 IEEE International Conference on Communications Workshops (ICC Workshops)*, 2018, pp. 1–6.

[12] H. Ren, C. Pan, K. Wang, Y. Deng, M. Elkashlan, and A. Nallanathan, "Achievable data rate for URLLC-enabled UAV systems with 3-D channel model," *IEEE Wireless Communications Letters*, vol. 8, no. 6, pp. 1587–1590, 2019.

[13] M. Ozger, M. Vondra, and C. Cavdar, "Towards beyond visual line of sight piloting of UAVs with ultra reliable low latency communication," in *Proceedings of 2018 IEEE Global Communications Conference (GLOBECOM)*, 2018, pp. 1–6.

[14] C. Pan, H. Ren, Y. Deng, M. Elkashlan, and A. Nallanathan, "Joint blocklength and location optimization for URLLC-enabled UAV relay systems," *IEEE Communications Letters*, vol. 23, no. 3, pp. 498–501, 2019.

[15] S. Kaul, R. Yates, and M. Gruteser, "Real-time status: how often should one update?" in *Proceedings of IEEE INFOCOM*, 2012, pp. 2731–2735.

[16] Y. Sun, E. Uysal-Biyikoglu, R. D. Yates, C. E. Koksal, and N. B. Shroff, "Update or wait: how to keep your data fresh," *IEEE Transactions on Information Theory*, vol. 63, no. 11, pp. 7492–7508, 2017.

[17] M. Costa, M. Codreanu, and A. Ephremides, "On the age of information in status update systems with packet management," *IEEE Transactions on Information Theory*, vol. 62, no. 4, pp. 1897–1910, 2016.

[18] J. Liu, X. Wang, B. Bai, and H. Dai, "Age-optimal trajectory planning for UAV-assisted data collection," in *Proceedings of IEEE INFOCOM 2018 - IEEE Conference on Computer Communications Workshops (INFOCOM WKSHPS)*, 2018, pp. 553–558.

[19] M. A. Abd-Elmagid and H. S. Dhillon, "Average peak age-of-information minimization in UAV-assisted IoT networks," *IEEE Transactions on Vehicular Technology*, vol. 68, no. 2, pp. 2003–2008, 2018.

[20] S. Zhang, H. Zhang, Z. Han, H. V. Poor, and L. Song, "Age of information in a cellular internet of UAVs: sensing and communication trade-off design," *IEEE Transactions on Wireless Communications*, 2020.

[21] X. Chen and S. S. Bidokhti, "Benefits of coding on age of information in broadcast networks," in *Proceedings of IEEE Information Theory Workshop (ITW)*, 2019, pp. 1–5.

[22] H. Sac, T. Bacinoglu, E. Uysal-Biyikoglu, and G. Durisi, "Age-optimal channel coding blocklength for an M/G/1 queue with HARQ," in *Proceedings of 2018 IEEE 19th International Workshop on Signal Processing Advances in Wireless Communications (SPAWC)*, 2018, pp. 1–5.

[23] A. Al-Hourani, S. Kandeepan, and S. Lardner, "Optimal LAP altitude for maximum coverage," *IEEE Wireless Communications Letters*, vol. 3, no. 6, pp. 569–572, 2014.

[24] R. Devassy, G. Durisi, P. Popovski, and E. G. Ström, "Finite-blocklength analysis of the ARQ-protocol throughput over the Gaussian collision channel," in *Proceedings of 2014 6th International Symposium on Communications, Control and Signal Processing (ISCCSP)*, 2014, pp. 173–177.

[25] M. Lubin, E. Yamangil, R. Bent, and J. P. Vielma, "Extended formulations in mixed-integer convex programming," in *Proceedings of International Conference on Integer Programming and Combinatorial Optimization*. Springer, 2016, pp. 102–113.

[26] R. Devassy, G. Durisi, G. C. Ferrante, O. Simeone, and E. Uysal-Biyikoglu, "Reliable transmission of short packets through queues and noisy channels under latency and peak-age violation guarantees," *IEEE Journal on Selected Areas in Communications*, vol. 37, no. 4, pp. 721–734, 2019.

[27] S. Xu, T. Chang, S. Lin, C. Shen, and G. Zhu, "Energy-efficient packet scheduling with finite blocklength codes: convexity analysis and efficient algorithms," *IEEE Transactions on Wireless Communications*, vol. 15, no. 8, pp. 5527–5540, Aug. 2016.